Fault detection and isolation in aircraft gas turbine engines. Part 2: validation on a simulation test bed

S Sarkar, M Yasar[†], S Gupta, A Ray[*], and K Mukherjee
Department of Mechanical Engineering, The Pennsylvania State University, University Park, Pennsylvania, USA

Abstract: The first part of this two-part paper, which is a companion paper, has developed a novel concept of fault detection and isolation (FDI) in aircraft gas turbine engines. The FDI algorithms are built upon the statistical pattern recognition method of symbolic dynamic filtering (SDF) that is especially suited for real-time detection and isolation of slowly evolving anomalies in engine components, in addition to abrupt faults. The FDI methodology is based on the analysis of time series data of available sensors and/or analytically derived variables in the gas path dynamics.

The current paper, which is the second of two parts, validates the algorithms of FDI, formulated in the first part, on a simulation test bed. The test bed is built upon an integrated model of a generic two-spool turbofan aircraft gas turbine engine including the engine control system.

Keywords: aircraft gas turbine engines, fault detection and isolation, symbolic dynamic filtering

1 INTRODUCTION

Detection of incipient faults and isolation of failure precursors are critical for safe and reliable operation of human-engineered complex systems. Therefore, it is necessary to develop fault detection and isolation (FDI) algorithms for enhanced reliability and to implement them for process monitoring during the service life of the system. With the advent of modern day technology, human-engineered systems have evolved as complex entities whose overall performance depend on several individual components that are interconnected with each other through a complex input–output structure and feedback paths. For example, performance of aircraft gas turbine engines gradually deteriorate due to degradation of different gas path components such as fan, compressor, combustor, and turbines [1].

Currently employed FDI tools for health monitoring of aircraft gas turbine engines vary widely in their complexity and applications and are primarily built upon both model-based [2, 3] and sensor-based analysis [4, 5]. However, it is often infeasible to develop sufficiently accurate and computationally efficient spatio-temporal models of thermo-fluid and structural system dynamics solely based on the fundamental principles of physics [6]. Similarly, sensor-based information alone may not be adequate for FDI if the available sensors are not consistently reliable (e.g. in the hot-section components of gas turbine) or if they are not sufficiently sensitive to small changes in the engine system behaviour. Therefore, early detection of small anomalies have to be inferred from a combination of time series analysis of the available sensor data and model-based information. As aircraft gas turbine engines consist of multiple interconnected components, even a single fault in one component produces an anomalous outputs that serve as input excitation to other healthy components. Therefore, gradual evolution of small anomalies (i.e. deviations from the nominal behaviour) in individual components may lead to cascaded faults because of strong input–output and feedback interconnections between the engine components and may eventually cause catastrophic failures and forced shutdown of the engine system.

The objective of this two-part paper is to develop and validate a novel methodology for FDI based on

---

[*]Corresponding author: Department of Mechanical Engineering, The Pennsylvania State University, 329 Reber Building, University Park, Pennsylvania 16802, USA. email: axr2@psu.edu
[†]Now at: Techno-Sciences, Inc., Beltsville, Maryland, USA

time series of pertinent sensor data and analytically derived variables [**7**, **8**]. The underlying concept of the FDI algorithms, presented in the first part [**8**] of this paper, are built upon the concept of symbolic dynamic filtering (SDF) [**4**, **9**, **10**] that is recently reported in literature as a pattern recognition tool. This paper, which is the second part, validates the proposed FDI concept on a simulation test bed of a generic two-spool turbofan engine [**11**, **12**]. The FDI algorithms are executable on commercially available inexpensive platforms in real-time and are implemented on the simulation test-bed.

This paper is organized in five sections and an appendix. Section 2 describes the simulation test bed of a generic aircraft gas turbine two-spool turbofan engine and the pertinent model equations are listed in 5.3. Section 3 presents implementation procedure of the *FDI* methodology, formulated in the first part [**8**]. Section 4 presents the pertinent results along with discussion on detection and isolation of single-component and multi-component faults. The two-part paper is summarized and concluded in section 5 along with recommendations for future research.

2 AIRCRAFT ENGINE SIMULATION TEST BED

This section describes the simulation test bed, consisting of an aircraft gas turbine engine model and its control system. The governing equations of the two-spool, low bypass turbofan engine model are derived in Appendix 2. Further details are available in technical literature on similar engine models, for example, Modular Aero Propulsion System Simulation (MAPSS) model [**12**, **13**] and the model of General Electric XTE-46 engine reported by Diao and Passino [**11**].

Following Fig. 1, the gas turbine engine system consists of compressor, combustor, and turbine subsystems that form the core of the engine model [**13**]. The core is also referred to as the gas generator because the output of the core is hot exhaust gas. In the turbofan engine, the engine core is surrounded by a fan in the front and an additional turbine at the rear. The fan and turbine are connected by an additional shaft. The fan shaft passes through the core shaft and this type of arrangement is called a two spool engine; one 'spool' for the fan, and another 'spool' for the core. The incoming air is captured by the engine inlet; a major part of the incoming air passes through the fan and continues on into the core compressor and then into the combustor, where it is mixed with fuel and combustion occurs. The hot exhaust passes through the core and fan turbines and then leaves out from the nozzle. This airflow is called the core airflow and the rest of the incoming air passes through the fan and bypasses, or goes around the engine. Parts of the thrust of the turbofan engine are generated by the core and the fan.

2.1 Dynamic model of the turbofan engine

The schematic of the engine model is depicted in Fig. 1 and the sensors and actuators are listed in Tables 1 and 2, respectively. The components of the engine model consist of a single stage high-pressure ratio fan with variable inlet stator vanes, booster with independent hub and tip stator vanes, high-pressure mixed flow compressor, double-annular combustor, high- and low-pressure turbines, afterburner, and nozzle components [**12**, **13**]. The components of the engine model and station numbering is provided in Fig. 1. The stations are numbered at the exit condition of each component starting from the flight conditions and inlet as the first station. The details are provided in Appendix 1. The health of the engine is described by
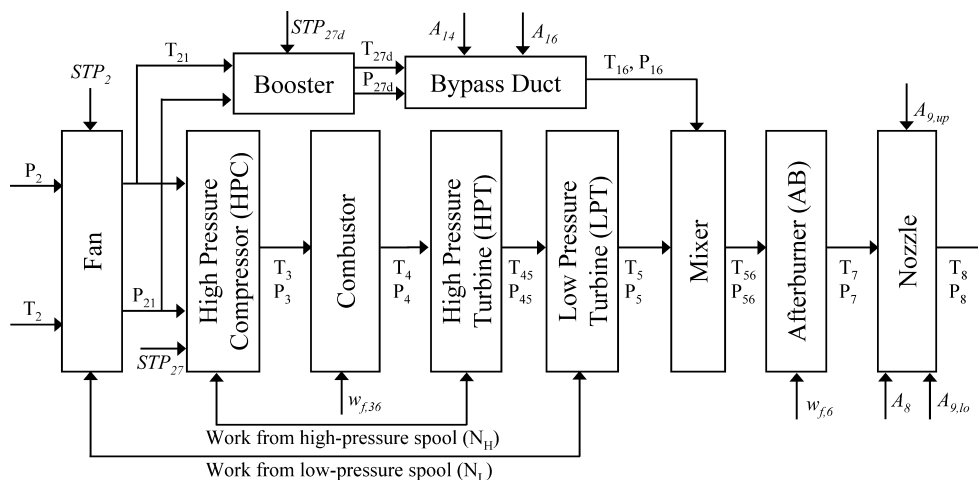

Fig. 1   Schematic of the TESM with labelled actuators (italics) and sensors

Table 1   Engine system sensors

Sensors	Description	Availability
P_2	Fan inlet pressure	CA
T_2	Fan inlet temperature	CA
N_L	Fan and LPT shaft speed	CA
P_{21}	Fan exit/HPC and booster inlet pressure	OA
T_{21}	Fan exit/HPC and booster inlet temperature	OA
N_H	HPC and HPT shaft speed	CA
P_{27d}	Booster exit pressure	OA
T_{27d}	Booster exit temperature	OA
P_{16}	Bypass duct exit pressure	OA
T_{16}	Bypass duct exit temperature	OA
P_3	HPC exit/combustor inlet pressure	CA
T_3	HPC exit/combustor inlet temperature	CA
P_4	Combustor exit/HPT inlet pressure	UA
T_4	Combustor exit/HPT inlet temperature	UA
P_{45}	HPT exit/LPT inlet pressure	OA
T_{45}	HPT exit/LPT inlet temperature	CA
P_5	LPT exit/mixer inlet pressure	OA
T_5	LPT exit/mixer inlet temperature	OA
P_6	Mixer exit/afterburner inlet pressure	OA
T_6	Mixer exit/afterburner inlet temperature	OA
P_7	Afterburner exit/nozzle inlet pressure	OA
T_7	Afterburner exit/nozzle inlet temperature	OA
P_8	Nozzle exit pressure	OA
T_8	Nozzle exit temperature	OA

CA ≡ Commercially available, OA ≡ Optionally available, UA ≡ Commercially unavailable

Table 2   Engine system actuators

Actuators	Description
STP_2	Fan variable inlet stator vane angle
A_1	Forward blocker door area
STP_{27}	High-pressure compressor stator vane angle
STP_{27d}	High-pressure booster hub stator vane angle
$w_{f,36}$	Combustor fuel flow
A_{16}	Aft variable bypass area
$w_{f,6}$	Afterburner fuel flow
A_8	Nozzle throat area
$A_{9,up}$	Upper nozzle exit area
$A_{9,lo}$	Lower nozzle exit area

the efficiency health parameter (ψ) and the flow health parameter (ζ) that are, in general, defined [**14**] as:

(a) $\psi \triangleq$ The ratio of actual enthalpy change and ideal enthalpy change;

(b) $\zeta \triangleq$ The ratio of tip rotor velocity and axial fluid flow velocity.

For six major components: (a) fan (ψ_F, ζ_F), (b) booster (ψ_B, ζ_B), (c) high pressure compressor (ψ_{HPC}, ζ_{HPC}), (d) combustor (ψ_C), (e) high pressure turbine (ψ_{HPT}, ζ_{HPT}), and (f) low pressure turbine (ψ_{LPT}, ζ_{LPT}) [**14**], the eleven health parameters affect the efficiency and flow of the respective components (see the engine model equations in 5.3). Note that there is no flow health parameter defined for combustor.

The engine model in this paper is similar to the NASA MAPSS model [**12**] and the model reported in [**11**]. The open-loop engine model has three state variables, namely, low-pressure spool speed,

high-pressure spool speed, and average temperature of the combustor wall structure. Together with ten actuators (see Fig. 1 and Table 2), each of which is modelled by a second order differential equation, total number of state variables associated with the augmented plant model is 23.

Given the inputs of throttle position, also known as power lever angle (PLA), and ambient conditions (e.g. altitude (a), Mach number (M), ambient temperature (T_{amb})), the interactively controlled component models at the simulation test bed compute non-linear dynamics of real-time turbofan engine operation. Both steady-state and transient operations are simulated in the continuous-time setting. Performance maps are used to provide steady-state representations of the engine's rotating components. Fluid momentum in the bypass duct and the augmentor, mass and energy storage within control volumes, and rotor inertias are also included to model transient operations.

2.2 Integration of the simulation model with the FDI system

In the present experimentation procedure, the engine simulation system (see details in section 2.1 and Appendix 2) and the FDI system (see details in the first part [**8**]) run on two computers connected via a network. The engine simulation system, which is a combination of the engine dynamic model and the engine controller, is hosted on the first computer. The engine model consists of non-linear differential and difference equations and supporting algebraic equations, and is designed for both steady-state and transient operations of a generic jet engine [**11**, **12**]. The engine simulation system is a stand-alone program with a gain-scheduled feedback controller. The simulation system is capable of generating time series data of all process variables of the gas turbine engine. Sensors and actuators that carry pertinent information for FDI are listed in Tables 1 and 2, and descriptions of the process variables therein follow Appendix 1.

The FDI system, that is hosted on the second computer, analyses the time series data of pertinent variables collected from the first computer over the communication channel. The data collected by the C++ wrapper program, which is installed over the core FORTRAN code of the engine simulation system, is transferred to the FDI system through an application protocol interface (API) that facilitates sending and receiving of message packages over the computer network through the standard transmission control protocol (TCP) and/or user datagram protocol (UDP) [**15**]. The data latency in this protocol interface is mainly due to the network communications and the typical value is found to be less than a fraction of millisecond. Since engine simulations use integration step sizes in

the order of 20 ms, the communication delays do not have a significant bearing on performance of the FDI algorithms that are implemented in the MATLAB 7.1 real-time environment.

3 VALIDATION OF FDI ALGORITHMS

This section describes planning and execution of simulation experiments for validation of FDI algorithms [8] on the test bed, described in section 2.

3.1 Implementation and validation of the FDI methodology

This section defines major components of the engine system as shown in Fig. 1. The inputs and outputs (see Tables 1 and 2) of these components, as needed for FDI analysis, are listed below.

1. Fan (F)
   (a) inputs: P_2, T_2, N_L, and STP_2
   (b) output: T_{21}
2. Booster (B)
   (a) inputs: P_{21}, T_{21}, and STP_{27d}
   (b) output: T_{27d}
3. High pressure compressor (HPC)
   (a) inputs: P_{21}, T_{21}, N_H, and STP_{27}
   (b) output: T_3
4. Combustor (C)
   (a) inputs: P_3, T_3, and $w_{f,36}$
   (b) output: T_4
5. High pressure turbine (HPT)
   (a) inputs: P_4, T_4, and N_H
   (b) output: T_{45}
6. Low pressure turbine (LPT)
   (a) inputs: P_{45}, T_{45} and N_L
   (b) output: T_5

The FDI methodology has been validated for the above six components under the assumption that all required sensors are available. However, due to the high temperature environment, P_4 and T_4 sensors may not be commercially available. In that case, a new subsystem C-HPT consisting of combustor and high pressure turbine could replace these two individual components for FDI analysis. The rationale is that, if P_4 and T_4 sensors are unavailable, the C-HPT subsystem will have sufficient input (i.e. P_3, T_3, N_H, and $w_{f,36}$) and output (i.e. T_{45}) information.

The source of faults in each of the six components is represented in terms of efficiency loss due to several factors related to malfunctioning (possibly due to structural damage), which leads to degraded performance and affects the gas-path sensor data. Several single component and multiple component faults are injected into the engine simulation system for different case studies. Faulty conditions are simulated

by reducing the health parameters, ψ and ζ, for each component under consideration. Imposition of these health parameters affects the actual efficiency and flow of the components in the simulation model of the engine system [12]. Note that, due to strong input–output and feedback interconnections between the engine components, deviation in the health parameters (from their nominal value) for a component not only degrades the performance of that component, but also may affect other components.

The nominal value of each health parameter is set to 1.0 under the healthy condition. Time series data of observed variables are analysed for detection of change in the signal, which provides relevant information for FDI. Faults were injected by reducing these parameter values below the nominal value (i.e. 1.0) for different components (see section 4 for details). For all the FDI analysis, the engine system model is excited with an input profile of the (PLA) having the mean value of $35°$ and frequency of 0.05 Hz as shown in Fig. 2. The ambient conditions are chosen to be at the sea-level (i.e. altitude ($a = 0.0$), Mach number ($M = 0$)) for the purpose of maintenance and fault monitoring by engineering personnel.

Simulation experiments on the engine test bed (see section 2) follow the concept of FDI laid out in the first part [8]. Accordingly, the engine simulation was executed for each of the six component models with faults injected as per different case scenarios (see section 4 for details) as well as for each of the six corresponding nominal component models (i.e. with no injected faults). The inputs for each component were kept the same for each component in the simulation of both the nominal models and fault-injected models as explained in the first part [8]. To include the effects of measurement noise in the engine components, zero mean additive Gaussian noise with standard deviation equal to 1 percent of the respective nominal value, is injected into the time series data for different sensors
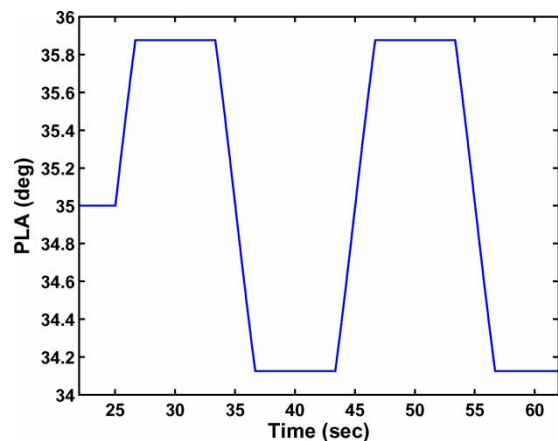

Fig. 2 Input Excitation for the PLA (*PLA*) Position

and analytically derived variables from the simulation model. The noise is not included in the nominal model. The critical issues in this procedure of simulation experimentation, as applied to each component, are delineated below.

1. Selection of an output (that may be either sensor generated or analytically derived) for each component and its nominal model.
2. Excitation of the nominal model of each component, for generation of compatible reference data, with the same inputs as the respective component.
3. Generation of anomaly measure, via the FDI algorithms using the SDF of output data and the respective nominal model data for each component.

After detecting and isolating a faulty component, the next task is to identify the range of the health parameters for each component as an extension of the current work reported in this paper. As explained in the first part [8], the task of degradation monitoring is divided into two parts: (a) assimilation of the fault information in the forward or analysis problem, and (b) fault range identification in the inverse or synthesis problem. Solution of the forward problem generates the probability distributions of the fault parameters off-line under an ensemble of physically admissible input and output variables. The inverse problem takes a statistical approach for online identification of the range of fault parameters at desired confidence levels. This concept has been experimentally validated for online estimation of fatigue life in polycrystalline alloys [5] and faulty parameters in active electronic circuits [16]. This work is under current investigation for identification of engine fault parameters and the results are expected to be reported in future publications.

3.2 Specifications of the SDF

SDF [9] has been used to generate patterns of anomalous behaviour (i.e. deviations from the nominal condition) for detection and isolation of faults in individual components of the engine system. Anomaly measure is quantitatively expressed as a (scalar) distance (e.g. statistical diversity) between two behaviour patterns generated by SDF as described in the first part [8]. The distance function is chosen to be the Euclidean norm of the difference between two pattern vectors. For symbol sequence generation, wavelet-based maximum entropy partitioning [10] has been used with the '*gaus*2' (i.e. Mexican Hat) basis function [17]; the alphabet size for partitioning is chosen to be $|\Sigma| = 8$ and the depth, $D = 1$, for construction of the finite state machine. Hence, the number of states in the finite state machine is $n = |\Sigma|^D = 8$. Based on the observed data sets, this choice of $|\Sigma|$

was made as a trade-off between anomaly detection capability and robustness to measurement noise. The SDF algorithms in this paper are implemented on the MATLAB platform and are interfaced with the engine simulation model for real-time operation.

The sampling frequency for data acquisition is chosen to be 50 Hz to match the updating rate of the digital controller, which is more than five times the highest signal frequency in the simulation model of the gas turbine engine. Hence, this sampling frequency satisfies the Nyquist criterion for avoidance of aliasing errors. The signal length r_{stop} for time series analysis is chosen from the stopping rule (see the first part [8])

$$r_{stop} \equiv \mathrm{int}\left(\frac{n}{\eta}\right)$$

where int($\bullet$) is the integer part of the real number $\bullet$, n is the number of states in the finite sate machine, and η is the allowed error tolerance ($0 < \eta \ll 1$). For $n = 8$ as stated above and choosing $\eta = 0.001$, the data length is selected to be 8000 points in the simulation runs, which is a conservative value. In majority of the cases, the convergence criterion for the stopping rule is satisfied much earlier and hence shorter signal lengths may be chosen.

4 RESULTS AND DISCUSSION

This section presents and discusses the results of experiments on the engine simulation test bed (see section 2) for validating the proposed detection and isolation algorithms for single-component and multi-component faults. Based on the procedure described in the first part [8], time series of the pertinent sensor data and analytically derived variables are generated from both (possibly anomalous) components and their respective nominal models for FDI in: (a) single components, and (b) multiple components.

4.1 Fault detection and isolation in single components

To demonstrate single-component *FDI*, the six identified components of the engine system are injected with a fault, one at a time, by reducing each of the respective efficiency health parameter (ψ) and the flow health parameter (ζ) from the nominal value of 1.0 to a degraded value of 0.99 that represents a small fault in the corresponding component. For this scenario, the six plates in Fig. 3 exhibit the exit temperature responses of the six components in the following order: (a) fan (*F*), (b) booster (*B*), (c) HPC, (d) combustor (*C*), (e) HPT, and (f) LPT, under the PLA excitation shown in Fig. 2. For the six components, the exit temperature responses of the nominal
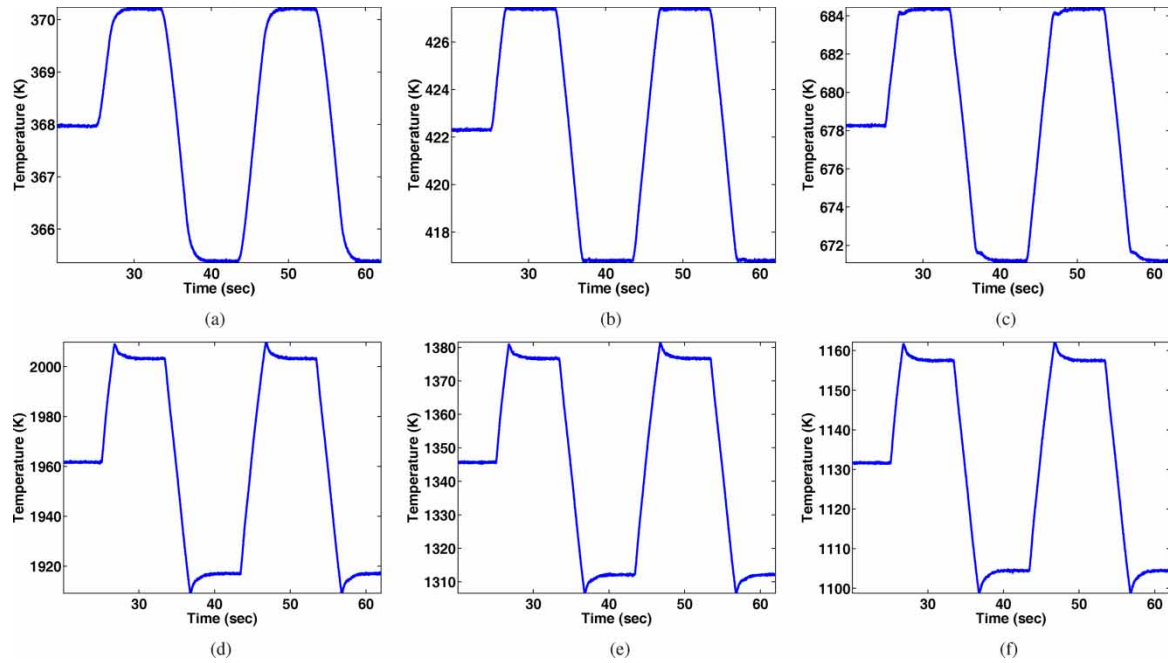
Fig. 3   Exit temperature response of the six engine components: (a) fan, (b) booster, (c) HP compressor, (d) combustor, (e) HPT, and (f) LPT
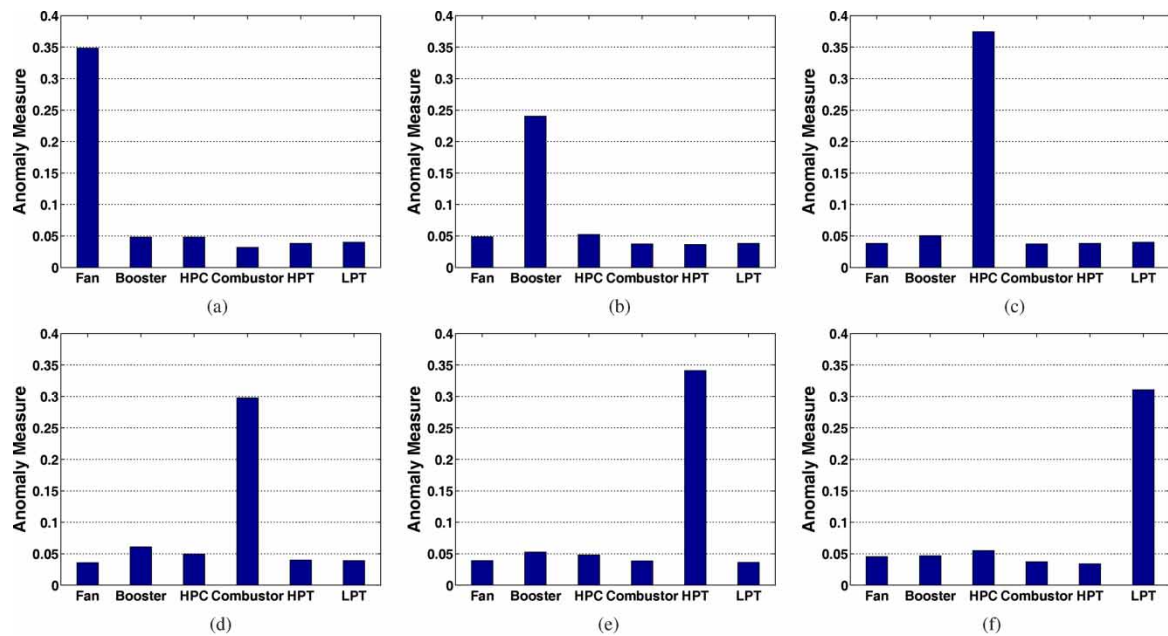

Fig. 4   Detection and isolation of faults in single components: (a) faulty fan, (b) faulty booster, (c) faulty HP compressor, (d) faulty combustor, (e) faulty HPT, and (f) faulty LPT

(i.e. $\psi = 1.0$ and $\zeta = 1.0$) models are too close to the respective responses in Fig. 3 to be distinguishable by visual inspection; hence, the nominal responses are not shown.

The vertical bars in each of the six plates in Fig. 4 represent the anomaly measure μ (refer to the first part [**8**]) for each component generated by analysis of the time series data of temperature response. It is

seen that the faulty component in each case has a high anomaly measure as compared to the remaining components that have relatively much smaller anomaly measure; non-zero values of anomaly measure in healthy components are attributed to noise. These bar plots demonstrate that it is possible to successfully detect and isolate the small fault (i.e. early detection) in a single component even if the data sets
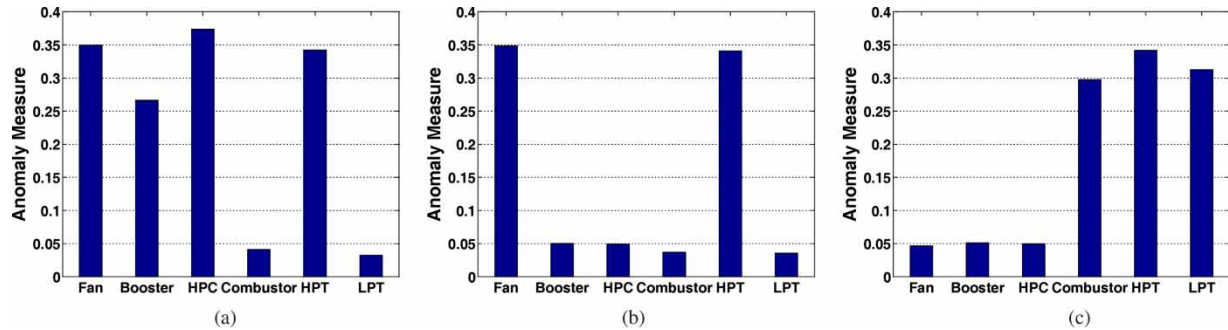
Fig. 5 Detection and isolation of identical faults in multiple components: (a) faulty fan, booster, HPC, HPT; (b) faulty fan, HPT; (c) faulty combustor, HPT, LPT

Table 3 Multiple component fault detection and isolation results using temperature data

Faulty components	Anomaly measure vector, μ					
	μ_{fan}	μ_{booster}	μ_{HPC}	$\mu_{\mathrm{combustor}}$	μ_{HPT}	μ_{LPT}
All components healthy	0.0416	0.0471	0.0458	0.0384	0.0344	0.0364
Fan, booster and LPT	**0.349**	**0.2387**	0.0518	0.035	0.0347	**0.3128**
Fan and HPT	**0.3484**	0.0502	0.0492	0.0372	**0.341**	0.0358
HPT and LPT	0.0512	0.0528	0.0531	0.0344	**0.3418**	**0.3135**
Fan, booster, HPC, combustor and HPT	**0.3495**	**0.254**	**0.3744**	**0.2987**	**0.3424**	0.0339
Booster, HPC and combustor	0.0449	**0.2351**	**0.3739**	**0.2985**	0.0322	0.0484

are noise-corrupted. The anomaly measure in Fig. 4 is a relative measure with respect to the reference condition of the nominal model; it does not represent anomalies at the absolute level.

4.2 Fault detection and isolation in multiple components

Figure 5 presents the results of detection and isolation of simultaneous faults in several components of a multi-component aircraft engine system. Faults were injected into multiple components of the engine system in the simulation test bed as a representation of the following scenario: components, detected with incipient faults, are not immediately repaired and such faulty components are allowed to accumulate.

4.2.1 Identical level of faults in multiple components

To construct this scenario, faults are simultaneously injected into multiple components by reducing the respective efficiency and flow health parameters, ψ and ζ from 1.0 to 0.99. The results were generated by analysing exit temperature data from the six components. Three plates in Fig. 5 exhibit three cases of randomly chosen faulty components:

(a) fan (F), booster (B), HPC, and HPT;
(b) fan and HPT;
(c) combustor (C), HPT and LPT.

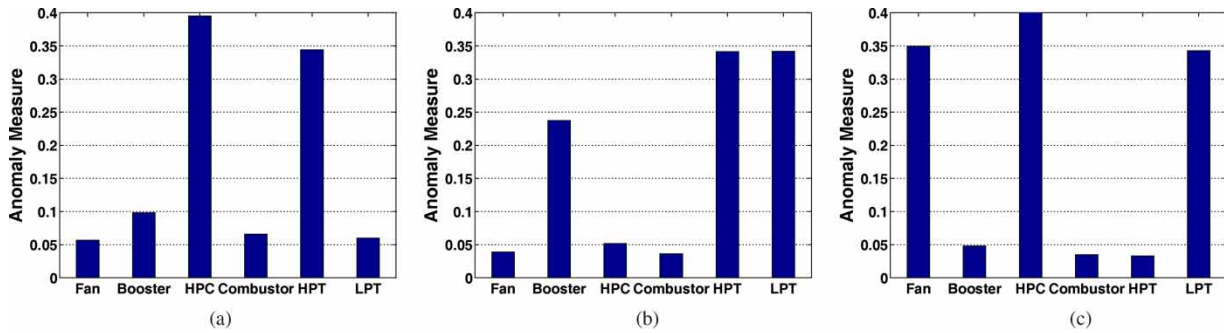The procedure for detection and isolation of multiple component faults is similar to that of the

single component faults. The effects of fault in one component could be pervasive throughout the engine system because of physical couplings among the components and also due to feedback and feed-forward control interactions. It is observed from the simulation results on the test bed that the SDF-based FDI algorithms successfully detect the small anomalies and correctly isolate the affected component(s) for both single-component and multiple-component faults.

Analytically derived variables can be used for FDI if appropriate sensor data are not available. In this context, several different scenarios with arbitrarily chosen multiple faulty components were investigated and compared. Tables 3 and 4 summarize the results for detection and isolation for these scenarios, with 1 percent reduction of the health parameters for each faulty component, based on the time series analysis of one sensor variable, namely, temperature and one analytically derived variable, namely, enthalpy, respectively. The anomaly measure vector $\boldsymbol{\mu}$ (see section 3 in the first part [8]) was obtained by analysing the time series data of individual components. The results in Tables 3 and 4 are presented in a matrix format, where a horizontal row demonstrates the anomaly measure $\boldsymbol{\mu}$ for all components for a particular multiple-component fault scenario and a vertical column provides the value μ_i for a particular component in different multiple-component fault scenarios.

It is seen that the faulty components exhibit significantly higher values of anomaly measure, which are indicated by bold scripts in Tables 3 and Table 4. For example, the second row in Table 3 indicates that

Table 4　Multiple component fault detection and isolation results using enthalpy data

Faulty components	Anomaly measure vector, μ					
	μ_{fan}	μ_{booster}	μ_{HPC}	$\mu_{\text{combustor}}$	μ_{HPT}	μ_{LPT}
All components healthy	0.0362	0.0506	0.0409	0.0339	0.0456	0.0332
Fan, booster and LPT	**0.3485**	**0.2384**	0.0451	0.0491	0.0378	**0.315**
Fan and HPT	**0.3495**	0.0473	0.0548	0.0408	**0.3452**	0.0454
HPT and LPT	0.031	0.0462	0.0484	0.0339	**0.346**	**0.3158**
Fan, booster, HPC, combustor and HPT	**0.3496**	**0.2652**	**0.3758**	**0.2905**	**0.3458**	0.0387
Booster, HPC and combustor	0.0457	**0.2444**	**0.3759**	**0.2901**	0.0353	0.0404

Fig. 6　Detection and isolation of non-identical faults in multiple components: (a) faulty HPC, HPT; (b) faulty booster, HPT, LPT; (c) faulty fan, HPC, LPT

fan, booster and LPT are simultaneously faulty, and the anomaly measure for each of these components shows a significant deviation from the nominal value and hence they are isolated as faulty.

It follows from the results presented in Tables 3 and Table 4 that analysis of either the temperature sensor data or the analytically derived enthalpy data can be successfully used for early detection and isolation of faults in multiple components. The rationale for having similar results is that enthalpy is a very strong function of temperature for gases at high temperature.

4.2.2　Non-identical level of faults in multiple components

To construct this scenario, non-identical faults are simultaneously injected into multiple components by either 1 percent or 2 percent reduction of the health parameters, ψ and ζ, for each faulty component. The results were generated by analysing exit temperature data from the six components. The three plates in Fig. 6 exhibit three cases of randomly chosen faulty components:

(a) HPC ($\psi = 0.98$ and $\zeta = 0.98$) and HPT ($\psi = 0.99$ and $\zeta = 0.99$);
(b) booster ($\psi = 0.99$ and $\zeta = 0.99$), HPT ($\psi = 0.99$ and $\zeta = 0.99$), and LPT ($\psi = 0.98$ and $\zeta = 0.98$);
(c) fan ($\psi = 0.99$ and $\zeta = 0.99$), HPC ($\psi = 0.98$ and $\zeta = 0.98$), and LPT ($\psi = 0.98$ and $\zeta = 0.98$).

The bar charts in Fig. 6 show that larger faults do not mask the smaller faults while there is no false indication of faults in the healthy components. It is to be noted that the anomaly measure shown in the bar charts in each of Figs 4 to 6 is a relative measure with respect to the corresponding component's reference condition and it does not represent anomalies at the absolute level. Therefore, the fault parameters cannot be directly estimated from these bar charts because of strong interactions among different components. This is an area of current investigation and would be reported in future publications.

5　SUMMARY, CONCLUSIONS, AND FUTURE WORK

This section summarizes both parts of the two-part paper with pertinent conclusions on efficacy of the proposed method for FDI in aircraft gas turbine engines. Areas of future research are also recommended to overcome the limitations of the proposed FDI method.

5.1　Summary of the two-part paper

This two-part paper addresses the issues of FDI for degradation monitoring of gas turbine engines in aircraft propulsion systems. It formulates a novel methodology for early detection of slowly evolving anomalies (i.e. deviations from the nominal behaviour) as well as abrupt faults in individual components. The

FDI algorithms are based on analysis of time series data observed from the instrumentation in engine components. The underlying concept is built upon SDF that has been recently reported in references [9] and [10] and is based on the principles of symbolic dynamics, statistical pattern recognition, and information theory. The FDI algorithms have been coded and validated for detection and isolation of incipient faults on a simulation test bed that incorporates a real-time model of a generic two-spool turbofan engine.

5.2 Pertinent conclusions

Experiments on the simulation test bed indicate that the proposed FDI method is capable of detecting and isolating incipient faults in one or more components of a gas turbine engine; in essence, the FDI method meets the challenge of identifying, at a very early stage, small anomalies that may eventually affect the performance of individual component(s) and (possibly) the entire engine. The existing instrumentation in a gas turbine engine are adequate for execution of the proposed FDI method except for a few cases which have been described earlier (e.g. possible unavailability of the sensors P_4 and T_4).

The software code of the FDI algorithm is executable in real time on commercially available computational platforms (e.g. PCs and laptops). Therefore, it is concluded that the FDI algorithm has the potential for assessment of individual component health status in an engine system, based on the filtered information derived from time series data of available sensors and analytically derived variables in the engine components. However, the FDI method must be validated on a commercial-scale engine before its incorporation within the testing and maintenance system software of gas turbine engines.

5.3 Recommendations for future research

Although the theory of the proposed FDI method is built upon rigorous principles, its software implementation requires application-specific relationships such as selection of the partitioning alphabet size [9] and wavelet basis functions and scale range [10]. A critical assumption, (that is trivially valid) in the simulation test runs, is availability of the engine component models under different input excitation. Such models may not be available for the necessary input conditions in an operating engine. To address the unresolved issues, future research is recommended in the following areas.

1. Theoretical research for enhancement of SDF, especially, on space partitioning: Fusion of multiple heterogeneous information from sensors and analytically derived variables into a single symbol sequence will facilitate real-time detection, isolation and estimation of pervasive faults.
2. System identification of engine component models under both normal and off-normal input excitations: This research involves development of new FDI tools that are not strongly dependent on the information of physics-based model(s) of engine gas path operations. For example, the reference behaviour of nominal engine components could be identified based on time series data of appropriate sensors and actuators [18]. As such data-driven nominal models of engine components could be obtained using black-box system identification such as statistical pattern recognition [19] and/or artificial neural networks techniques [20, 21].
3. Fault estimation: Quantitative evaluation of incipient faults in gas turbine engine components will facilitate health monitoring and preventive maintenance of the aircraft propulsion system.
4. Validation of the FDI algorithm on the test bed of an operating engine: This experimental research is an extension of what have been done on the engine simulation test bed. The results of this research will provide a proof of concept for detection and isolation of faults in gas turbine engines as needed for integrated vehicle health management (IVHM) and integrated resilient aircraft control (IRAC).

REFERENCES

1 **Razak, A. M. Y.** and **Carlyle, J. S.** An advanced model based health monitoring system to reduce gas turbine ownership cost. ASME Turbo Expo 2000, Munich, Germany, 2000, paper no. ASME-2000-GT-627.
2 **Volponi, A. J., DePold, H., Ganguli, R.,** and **Chen, D.** The use of Kalman filter and neural network methodologies in gas turbine performance diagnostics: a comparative study. ASME Turbo Expo 2000, Munich, Germany, 2000, paper no. ASME-2000-GT-547.
3 **Moller, J. C., Litt, J. S.,** and **Guo, T. H.** Neural network-based sensor validation for turboshaft engines. In 34th Joint Propulsion Conference cosponsored by AIAA, ASME, SAE, and ASEE, Cleveland, OH, USA, 1998, paper no. AIAA-98-3547.
4 **Gupta, S., Ray, A.,** and **Keller, E.** Symbolic time series analysis of ultrasonic data for early detection of fatigue damage. *Mech. Syst. Signal Process.*, 2007, **21**(2), 866–884.

5 **Gupta, S.** and **Ray, A.** Real-time fatigue life estimation in mechanical systems. *Meas. Sci. Technol.*, 2007, **18**(7), 1947–1957.

6 **Badii, R.** and **Politi, A.** *Complexity, hierarchical structures and scaling in physics*, 1997 (Cambridge University Press, Cambridge, UK).

7 **Simani, S., Fantuzzi, C.,** and **Patton, R.** *Model-based fault diagnosis in dynamical systems using identification techniques*, 2003 (Springer-Verlag, London, UK).

8 **Gupta, S., Ray, A., Sarkar, S.,** and **Yasar, M.** Fault detection and isolation in aircraft gas turbine engines. Part 1. Underlying concept. *Proc. IMechE, Part G: J. Aerospace Engineering*, 2008, **222**(G3), 307–318 (this issue).

9 **Ray, A.** Symbolic dynamic analysis of complex systems for anomaly detection. *Signal Process.*, 2004, **84**(7), 1115–1130.

10 **Rajagopalan, V.** and **Ray, A.** Symbolic time series analysis via wavelet-based partitioning. *Signal Process.*, 2006, **86**(11), 3309–3320.

11 **Diao, Y.** and **Passino, K. M.** Stable fault-tolerant adaptive fuzzy/neural control of a turbofan engine. *IEEE Trans. Control Syst. Technol.*, 2001, **9**(3), 494–509.

12 **Parker, K. I.** and **Guo, T. H.** Development of a turbofan engine simulation in a graphical simulation environment. In JANNAF Aero-Propulsion Subcommittee Meeting, Destin, FL, USA, 2002.

13 **Adibhatla, S.** and **Johnson, K. L.** Evaluation of nonlinear PSC algorithm on a variable cycle engine. In Proceedings of the AIAA 29th Joint Propulsion Conference and Exhibit, Monterey, CA, USA, 1993.

14 **Kobayashi, T.** and **Simon, D. L.** A hybrid neural network-genetic algorithm technique for aircraft engine performance diagnostics. In 37th Joint Propulsion Conference and Exhibit cosponsored by the AIAA, ASME, SAE, and ASEE, Salt Lake City, Utah, 2001, paper no. AIAA 2001-3763.

15 **Tanenbaum, A. S.** *Computer networks*, 4th edition, 2003 (Prentice Hall PTR, Upper Saddle River, NJ, USA).

16 **Rajagopalan, V., Chakraborty, S.** and **Ray, A.** Estimation of slowly-varying parameters in nonlinear systems via symbolic dynamic filtering. *Signal Process.*, 2008, **88**(2), 339–348.

17 **Mallat, S.** *A wavelet tour of signal processing*, 2nd edition, 1998 (Academic Press, Boston, MA, USA).

18 **Mushini, R.** and **Simon, D.** On optimization of sensor selection for aircraft gas turbine engines. In Proceedings of the 18th International Conference on Systems Engineering (ICSENG '05), Las Vegas, ND, USA, 2005.

19 **Duda, R. O., Hart, P. E.,** and **Stork, D. G.** *Pattern classification*, 2001 (John Wiley, New York, USA).

20 **Bishop, C. M.** *Neural networks for pattern recognition*, 1995 (Oxford University Press, New York, NY, USA).

21 **Hagan, M. T., Demuth, H. B.,** and **Beale, M. H.** *Neural network design*, 1996 (PWS Publishing, Boston, MA, USA).

APPENDIX 1

Notation

a	altitude
A	cross-sectional area
c_p	specific heat at constant pressure
c_v	specific heat at constant volume
CPR	compressor pressure ratio
f/a	fuel–air ratio
F	thrust
h	specific enthalpy
J	mechanical equivalent of heat
k	stall constant
M	Mach number
N	rotational spool speed
NPR	nozzle pressure ratio
P	total pressure
PW	power
Q	fuel heating value
R	gas constant
SM	stall margin
STP	stator vane angle
T	absolute temperature
TPR	turbine pressure ratio
V	velocity
w	mass flow rate
W	work
γ	ratio of specific heats
ζ	flow health parameter
η	efficiency of a component
θ	normalized ambient (absolute) temperature
μ	anomaly measure
ψ	efficiency health parameter

Subscripts

a	air
amb	ambient
B	booster
C	combustor
f	fuel
F	fan
G	gross
H	high-pressure spool
L	low-pressure spool
N	net
ram	ram
s	static
1	engine inlet
2	fan inlet
3	high-pressure compressor exit
4	combustor exit
5	low-pressure turbine exit
7	afterburner exit
8	nozzle exit
16	bypass duct exit
21	fan exit
27d	booster exit
45	high-pressure turbine exit
56	mixer exit

APPENDIX 2

Governing equations of the engine model

This appendix succinctly derives the governing equations of the simulation model of a generic two-spool, low-bypass turbofan engine [**12**] as described in section 2. Performance maps have been used extensively in the simulator to provide steady-state representations of the engine's rotating components. Fluid momentum in the bypass duct and the augmentor, mass and energy storage within control volumes, and rotor inertias are also included to provide transient capability. For completeness of the paper, the pertinent model equations of the major components of the engine system are provided below in simplified forms.

Flight and conditions inlet

Gas turbine engines have an inlet for free stream air flowing into the engine. The following equations define the flight conditions and inlet model

$$P_{\text{amb}} = f_1(a)$$
$$T_{\text{amb}} = f_2(a)$$

where f_1 and f_2 are curve-fitted functions that are generated from atmospheric data. The equations for pressure, temperature, and enthalpy at the fan inlet are given by

$$P_2 = P_{\text{amb}}\phi(M)\left[1.0 + \frac{(\gamma_1 - 1)M^2}{2}\right]^{\gamma_1/(\gamma_1 - 1)}$$
$$T_2 = T_{\text{amb}}\left[1.0 + \frac{(\gamma_1 - 1)M^2}{2}\right]$$
$$h_2 = c_p T_2$$

where

$$\phi = 1.0 \quad \text{if} \quad M \leqslant 1.0$$
$$= 1.0 - 0.075(M - 1.0)^{1.35} \quad \text{if} \quad M > 1.0$$
$$\gamma_1 = 1.4$$

Fan

Fan performance is represented by a set of performance maps. Separate maps are used for the tip and hub sections of the fan. These maps are assumed to represent fan performance with variable geometry at nominal and scheduled positions. Map-generated, fan-corrected airflow is adjusted to account for off-schedule geometry effects. The following equations

describe the fan model

$$P_{21} = P_2 f_3\left(\frac{P_2}{P_{\text{amb}}}, \sqrt{\theta_2}, N_{\text{L}}\right)$$
$$h_{21} = h_2 + 5.858 \times 10^{-5} T_2 f_4(\psi_{\text{F}}, \zeta_{\text{F}})$$
$$T_{21} = f_5(h_{21})$$
$$\eta_{\text{F}} = \frac{h_{21} - h_2}{h_{21}}$$
$$w_{21} = f_6\left(\sqrt{\theta_2}, \frac{P_{21}}{P_{amb}}, N_L\right)$$
$$\text{PW}_{\text{F}} = (h_{21} - h_2)w_{21}$$
$$\text{SM}_{\text{F}} = \left(k_2 \frac{w_{21}}{P_{21}/P_{\text{amb}}} - 1\right) \times 100$$

where f_3, f_4, f_5, and f_6 are the performance maps of the fan, which are provided in tabular formats in the engine simulation program; and k_2 is the fan stall line parameter due to distortion.

Booster and high-pressure compressor

Modern large turbofan engines usually have axial compressors. Performance maps are used for the compressor with a shift in the corrected airflow based on off-schedule values of variable-geometry position. The following equations describe the booster model and the high pressure compressor model

$$h_{27d} = 5.858 \times 10^{-5} \cdot f_7(\psi_{\text{B}}, \zeta_{\text{B}})$$
$$\eta_{\text{B}} = \frac{h_{27d} - h_{21}}{h_{27d}}$$
$$w_{27d} = f_8\left(\sqrt{\theta_{27d}}, \frac{P_{27d}}{P_{\text{amb}}}, N_{\text{H}}\right)$$
$$\text{PW}_{\text{B}} = (h_{27d} - h_{21})w_{27d}$$
$$\text{SM}_{\text{B}} = \left(k_{27d} \frac{w_{27d}}{(P_{27d}/P_{\text{amb}})} - 1\right) \times 100$$

where f_7 and f_8 are performance maps of the booster, which are provided in tabular formats in the engine simulation program; and k_{27d} is the booster stall line parameter due to distortion.

$$h_3 = 5.858 \times 10^{-5} f_9(\psi_{\text{HPC}}, \zeta_{\text{HPC}})$$
$$\text{CPR} = \left(\frac{h_3}{0.23995} + 1\right)^{\gamma_{21}/(\gamma_{21} - 1)}$$
$$P_3 = P_{21}\text{CPR}$$
$$\frac{T_3}{T_{21}} = \left(\frac{P_3}{P_{21}}\right)^{(\gamma_{21} - 1)/\gamma_{21}}$$
$$\eta_{\text{HPC}} = \frac{h_3 - h_{21}}{h_3}$$

$$w_3 = f_{10}\left(\sqrt{\theta_3}, \frac{P_3}{P_{\text{amb}}}, N_{\text{H}}\right)$$

$$\text{PW}_{\text{HPC}} = (h_3 - h_{21})w_3$$

$$\text{W}_{\text{HPC}} = \frac{c_{\text{p}}T_{21}}{\eta_3}\left[\text{CPR}^{(\gamma_{21}-1)/\gamma_{21}} - 1\right]$$

$$\text{SM}_{\text{HPC}} = \left(k_3 \frac{w_3}{(P_3/P_{\text{amb}})} - 1\right) \times 100$$

where f_9 and f_{10} are performance maps of the high pressure compressor, which are provided in tabular formats in the engine simulation program; and k_3 is the compressor stall line parameter due to distortion.

Combustor

Total pressure losses are included in the models of main combustor, bypass duct, mixer entrance, and augmentor. Heat generation associated with the burning of fuel in the main combustor is assumed to take place at a constant combustor volume

$$P_4 = P_3 - 7.57 \times 10^{-4} w_3^2 \frac{T_3}{P_3}$$

$$h_4 = \frac{h_3 + (f/a)_4 \eta_{\text{C}} Q}{\left[1 + (f/a)_4\right]}$$

$$T_4 = \frac{h_4}{c_{\text{p}}}$$

The combustor health parameter (ψ_{C}) is a scaling factor for combustor efficiency η_{C}.

Power turbines

In the two-spool turbofan engine, high-pressure and low-pressure turbines produce engine thrust and also drive the compressor and the fan, respectively. Performance of the high-pressure and low-pressure turbines is represented by performance maps. Cooling bleed for each turbine is assumed to re-enter the cycle at the turbine discharge although a portion of each bleed is assumed to contributed to the power generated by the turbines

$$\text{TPR}_{\text{HPT}} = \frac{P_{45}}{P_4}$$

$$\frac{T_{45}}{T_4} = \left(\frac{P_{45}}{P_4}\right)^{(\gamma_4-1)/\gamma_4}$$

$$h_{45} = c_{\text{p}}T_{45}$$

$$\eta_{\text{HPT}} = f_{11}(h_{45}, h_4, \psi_{\text{HPT}})$$

$$w_{45} = f_{12}\left(N_{\text{H}}, \frac{\sqrt{T_{45}}}{P_4}, \zeta_{\text{HPT}}\right)$$

$$W_{\text{HPT}} = h_{45} - h_4 = c_{\text{p}}(T_{45} - T_4)$$

$$\text{PW}_{\text{HPT}} = (h_{45} - h_4)w_{45}$$

where f_{11} and f_{12} are performance maps of the high pressure turbine, which are provided in tabular formats in the engine simulation program

$$\text{TPR}_{\text{LPT}} = \frac{P_5}{P_{45}}$$

$$\frac{T_5}{T_{45}} = \left(\frac{P_5}{P_{45}}\right)^{(\gamma_{45}-1)/\gamma_{45}}$$

$$h_5 = c_{\text{p}}T_5$$

$$\eta_{\text{LPT}} = f_{13}(h_5, h_{45}, \psi_{\text{LPT}})$$

$$w_5 = f_{14}\left(N_{\text{L}}, \frac{\sqrt{T_5}}{P_{45}}, \zeta_{\text{LPT}}\right)$$

$$W_{\text{LPT}} = h_5 - h_{45} = c_{\text{p}}(T_5 - T_{45})$$

$$\text{PW}_{\text{LPT}} = (h_5 - h_{45})w_5$$

where f_{13} and f_{14} are performance maps of the low pressure turbine, which are provided in tabular formats in the engine simulation program.

Nozzle

The nozzle is located downstream of the power turbines and does no work on the flow. A convergent–divergent nozzle configuration is assumed. The following equations describe the nozzle model

$$\text{NPR} = \frac{P_8}{P_{\text{amb}}}$$

$$\frac{T_8}{T_{\text{amb}}} = \left(\frac{P_8}{P_{\text{amb}}}\right)^{(\gamma_8-1)/\gamma_8}$$

$$h_8 = h_{8\text{s}} + \frac{V_8^2}{2\eta_8}$$

$$V_8 = \sqrt{2\eta_8 c_p T_8 \left[1 - \left(\frac{1}{\text{NPR}}\right)^{(\gamma_8-1)/\gamma_8}\right]}$$

$$F_{\text{G}} = \frac{w_8(1.0244 - 0.6067(f/a)_6)V_8}{32.17}$$

$$F_{\text{ram}} = w_2 M 1.5238\sqrt{T_{\text{amb}}}$$

$$F_{\text{N}} = F_{\text{G}} - F_{\text{ram}}$$